

APPLICATION OF TENSION SOFTENING CURVES TO INVESTIGATE THE SHEAR CARRIED BY FIBERS IN VARIOUS FIBER REINFORCED CONCRETE BEAMS

PITCHA JONGVIVATSAKUL^{*}, KOJI MATSUMOTO[†], KEN WATANABE^{††}
AND JUNICHIRO NIWA[†]

^{*} Department of Civil Engineering
Tokyo Institute of Technology, Tokyo, Japan
e-mail: jongvivatsakul.p.aa@m.titech.ac.jp

[†] Department of Civil Engineering
Tokyo Institute of Technology, Tokyo, Japan
e-mail: matsumoto.k.ar@m.titech.ac.jp, jniwa@cv.titech.ac.jp

^{††} Railway Technical Research Institute
Concrete Structures, Structures Technology Division, Tokyo, Japan
e-mail: wataken@rtri.or.jp, web page: <http://www.rtri.or.jp/eng/index.html>

Key words: Shear Carried by Fibers, Fiber Reinforced Concrete, Tension Softening Curves, Crack Surface Displacement, Diagonal Crack Length, Image Analysis System

Abstract: Shear resisting mechanisms and the diagonal cracking behavior of fiber reinforced concrete (FRC) beams with stirrups were discussed in this paper. Five FRC beams with various types of fibers, which were 30-mm and 60-mm long and made of steel, polypropylene, polyvinyl alcohol, and polyethylene terephthalate, were tested. The method to evaluate shear carried by fibers in FRC beams using tension softening curves was presented. The tension softening curve was used to investigate the force transferred across the diagonal crack from its width, which was measured using the image analysis system. The shear carried by fibers was calculated using the proposed method. In addition, the cracking of FRC beams was studied.

1 INTRODUCTION

The use of fibers as shear reinforcement has focused exclusively on steel fibers. Several researchers [1-3] have proposed the equations of shear capacity for steel fiber reinforced concrete beams. However, these studies have been performed without transverse reinforcement. Recently, synthetic fibers have become more attractive because of the effectiveness with which they improve shear strength [4] and their relatively less cost when compared with that of steel fibers. Nevertheless, the influence of steel and synthetic fibers on the shear resisting

mechanism of fiber reinforced concrete (FRC) beams with stirrups has not been completely understood.

In the Japanese design guidelines for reinforced concrete piers with steel fibers [5], steel fibers have been considered for the shear reinforcement of concrete structures. The increment in shear strength by mixing steel fibers has been expressed as a value κ , which has been defined as the ratio of shear carried by steel fibers to the shear carried by concrete, and it was equal to 1.0 in the guidelines. However, the post-cracking behavior of FRC beams has not been considered in the design

guidelines.

The method to evaluate shear carried by steel fibers of FRC beams with stirrups was proposed by the authors (Jongvivatsakul et al. [6]). The proposed method considered the post-cracking behavior of FRC beams with stirrups by applying the concept of fracture mechanics with the shear behavior of FRC beams. The tension softening curve—one of the parameters in fracture mechanics—was used to explain the post-cracking behavior of FRC beams. The crack surface displacement of the diagonal crack, which was the total displacement of the crack in the direction of the principal tensile strain, was measured by the image analysis system. The stress transferred across the diagonal crack of the FRC beams was calculated using the relationship between the tension softening curve and crack surface displacement. Moreover, shear force carried by fibers has been calculated.

This study intends to investigate the shear carried by steel and synthetic fibers of FRC beams with stirrups by using tension softening curves. The shear resisting mechanism of five FRC beams with stirrups and various types of fibers (i.e., material type and length) was examined. In addition, the diagonal cracking behavior (i.e., the crack surface displacement, diagonal crack length, and angle of diagonal cracks) and tensile stress transferred across the diagonal crack were discussed. The method to evaluate shear carried by fibers using tension softening curves [6] was verified to confirm the applicability of those curves in investigating shear capacity of FRC beams with stirrups and various fibers.

2 EXPERIMENTAL PROCEDURE

2.1 Material

The materials used in this study were high-strength Portland cement, fine aggregates, coarse aggregates, and high-performance air-entraining (AE) water-reducing agent. Table 1 shows the mixture proportion for concrete.

Five types of fibers were incorporated into

Table 1: Mixture proportion for concrete

G_{max} (mm)	W/C	Unit weight (kg/m ³)				
		W	C	S	G	SP
20	0.35	165	471	917	790	5.2

G_{max} = maximum size of the coarse aggregate,
 W = water, C = cement, S = fine aggregate,
 G = coarse aggregate, SP = high-performance air-entraining (AE) water-reducing agent

Table 2: Properties of fibers

Name	L (mm)	ϕ (mm)	Density (kg/m ³)	Tensile strength (MPa)	E (GPa)	Shape of the end
SF30	30	0.62	7850	1050	210	Hooked
SF60	60	0.90	7850	1050	210	Hooked
PP	30	1.6×0.6	910	470	15	Straight
PVA	30	0.66	1300	960	23	Straight
PET	30	0.70	1370	460	5.8	Straight

L = Length, ϕ = Diameter, and E = Elastic modulus

concrete, including steel fibers with lengths of 30 mm (SF30) and 60 mm (SF60), polypropylene fibers (PP), polyvinyl alcohol fibers (PVA), and polyethylene terephthalate fibers (PET). Pictures of the fibers are shown in Fig. 1, and their properties are summarized in Table 2. The volume fraction of fibers was equal to 1.0% of the full volume of the concrete in all specimens.

The longitudinal reinforcing bars were made of deformed steel having 25.4-mm nominal diameter and 1006-N/mm² yield strength. The stirrups made of deformed steel that was 6.35 mm in nominal diameter were arranged as the shear reinforcement. The yield strength was 315 N/mm². Two round bars of 6-mm diameter were used as compression bars with yield strength of 304 N/mm².

2.2 Specimens

Figure 2 shows the dimension and reinforcing bar arrangement of a FRC beam. The shear span (a) was 700 mm, and the effective depth (d) was 250 mm. The ratio of shear span to the effective depth (a/d) was 2.8. The longitudinal reinforcement ratio (p_w) was 2.7%. All specimens were controlled such that they would fail in the left shear span by providing fewer stirrups in the left shear span,

as shown in Fig. 2. The stirrup ratio in the test span (r_w) was 0.30% in all specimens. Five FRC beams were prepared with different types of fibers. The specimens were named according to the type of fibers used in the beams.

2.3 Loading setup and instrumentation

Specimens were subjected to a four-point bending with a simply-supported condition, as illustrated in Fig. 2. Steel plates were placed on the pin-hinge supports and loading points. Figure 2 shows the detailed loading arrangement along with the locations of loading points and strain gauges.

The measuring parameters were the applied load, displacements of mid-span and supporting points using four transducers, and the strain of the longitudinal steel bars and stirrups. The strain of the longitudinal steel bars was measured at mid-span using strain gauges, whereas the strains of stirrups were measured at the locations where the diagonal crack was expected to occur, as shown in Fig. 2.

2.4 Measurement of crack surface displacement and diagonal crack length

Crack surface displacement (u) was measured from the image analysis system developed by Watanabe et al. [7]. Crack

surface displacement (u) is defined as the total displacement of cracks in the direction of principal tensile strain (β), which is the direction of the crack's movement, as shown in Fig. 3. Figure 4 presents a photograph of the loading test with the analysis system. To analyze the image, red targets of 5-mm diameter were attached on the specimen surface with an interval of 20 mm. During the loading test, photographs of the specimen were captured for every 5 kN of shear force by using three digital cameras fixed on tripods. The image analysis system can investigate the coordinates of the red targets throughout the test span. As a result, the crack surface displacement can be calculated.

Because the diagonal crack was expected to open rapidly near the peak load, some photographs were captured near the peak load with short time intervals to capture the exact behavior at the peak.

Moreover, the length and angle of the diagonal crack were measured from the visible diagonal crack at the peak load by using the software system, which supports analytical functions ranging from the image measurement to statistical data processing. Calibration was performed to define the length of one pixel in the image for converting the measurement data in pixels to actual lengths. In addition, the images captured for the measurements of crack surface displacements

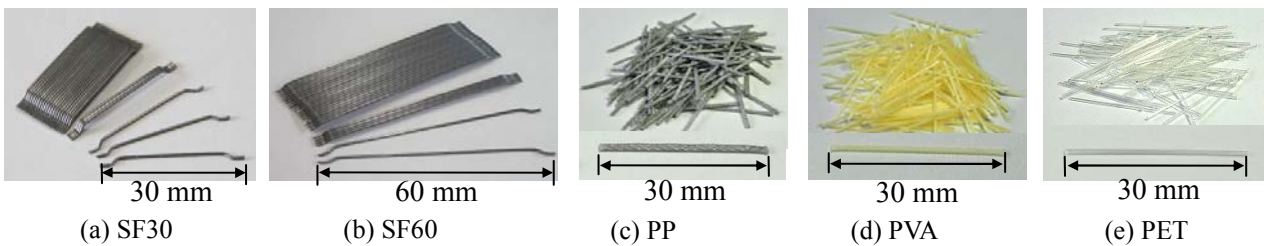


Figure 1: Types of Fibers

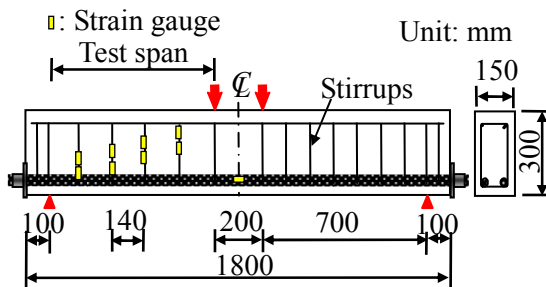


Figure 2: Detailed diagram of a FRC beam

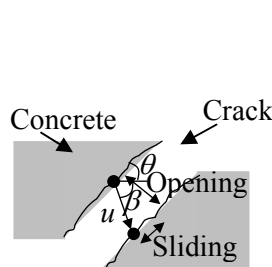


Figure 3: Definition of u

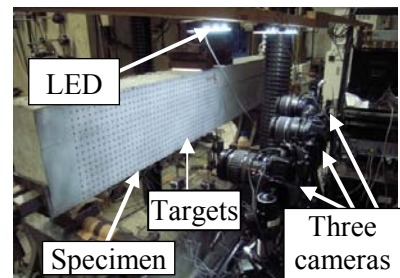


Figure 4: Preparation of the loading test

were used to measure crack length and the angle of diagonal cracks at the peak.

3 TENSION SOFTENING CURVES

The tension softening curves were used to investigate stress transferred across the diagonal crack of FRC beams. The curves were obtained from the bending tests of notched beams with a dimension of $100 \times 100 \times 400$ mm, following the standard of the Japan Concrete Institute [8]. The tension softening curves of five types of fiber reinforced concrete are shown in Fig. 5. Table 3 lists the compressive strength and fracture energy of the concrete measured by notched beam tests. Using a least-squares data-fitting procedure, the shape of bilinear curves of the tension softening diagram can be obtained as shown in Table 3.

As observed in Fig. 5, the tension softening behavior varied depending on the type of

fibers. SF60 can resist the highest stress in the post-cracking region. Steel fibers (SF30 and SF60) can transfer higher stress than that by synthetic fibers (PP, PVA, and PET). There were two mechanisms in which the stress transferred between crack surfaces was lost. SF30 and SF60 failed in the pulled-out mechanism, whereas PP, PVA, and PET exhibited both pulled-out and cut-off mechanisms. Because the tensile strength of steel fibers was comparatively greater than their bond strength, pull-out failure occurred.

4 CALCULATION OF SHEAR FORCES AND EVALUATION OF SHEAR CARRIED BY FIBERS

4.1 Calculation of shear forces in FRC beams

Considering the force acting at the diagonal crack in a FRC beam subjected to point loads (Fig. 6), shear force is resisted by shear

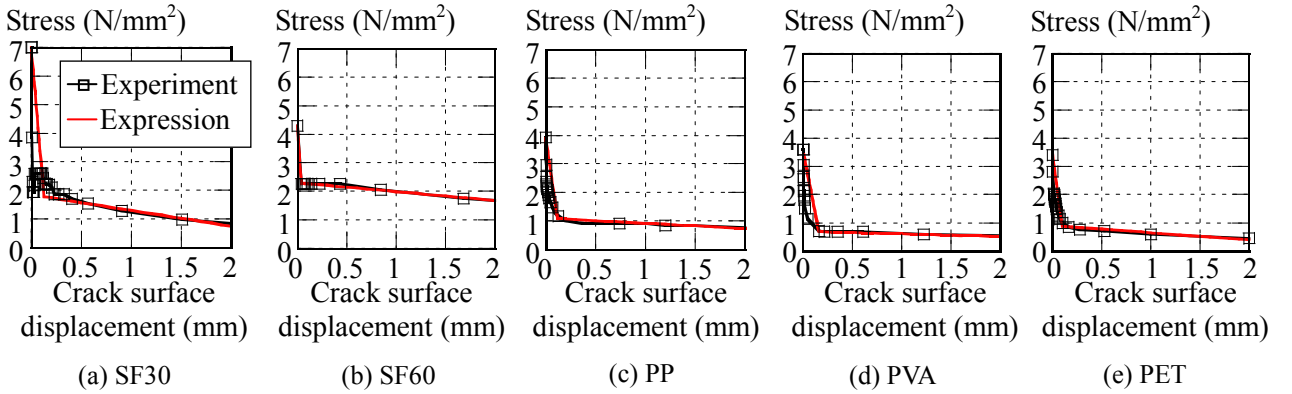


Figure 5: Tension softening curves

Table 3: Properties and expression of tension softening curves

Type	f'_c (N/mm ²)	f_t (N/mm ²)	G_F (N/mm)	Expression
SF30	56.6	3.6	4.24	$\sigma = \begin{cases} 7.0 - 40.2u & \text{for } u < 0.13 \text{ mm} \\ 1.85 - 0.55u & \text{for } u \geq 0.13 \text{ mm} \end{cases}$
SF60	55.9	3.4	8.82	$\sigma = \begin{cases} 4.3 - 50.5u & \text{for } u < 0.04 \text{ mm} \\ 2.3 - 0.31u & \text{for } u \geq 0.04 \text{ mm} \end{cases}$
PP	58.8	3.9	3.02	$\sigma = \begin{cases} 3.9 - 23.5u & \text{for } u < 0.12 \text{ mm} \\ 1.1 - 0.18u & \text{for } u \geq 0.12 \text{ mm} \end{cases}$
PVA	59.9	3.6	2.34	$\sigma = \begin{cases} 3.6 - 18.2u & \text{for } u < 0.16 \text{ mm} \\ 0.7 - 0.09u & \text{for } u \geq 0.16 \text{ mm} \end{cases}$
PET	61.5	3.3	2.89	$\sigma = \begin{cases} 3.4 - 25.2u & \text{for } u < 0.10 \text{ mm} \\ 0.9 - 0.25u & \text{for } u \geq 0.10 \text{ mm} \end{cases}$

f'_c : compressive strength, f_t : tensile strength, G_F : fracture energy

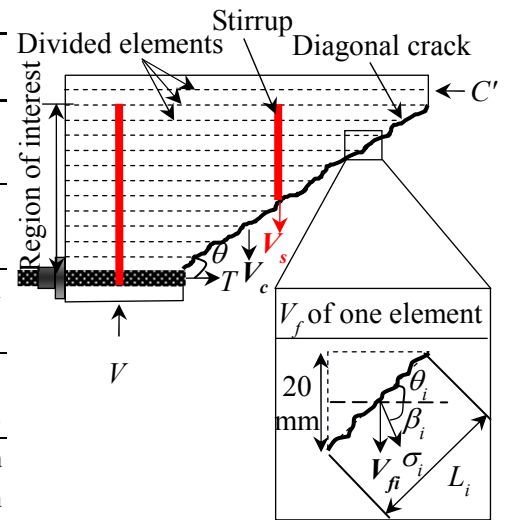


Figure 6: Free body diagram of a FRC beam

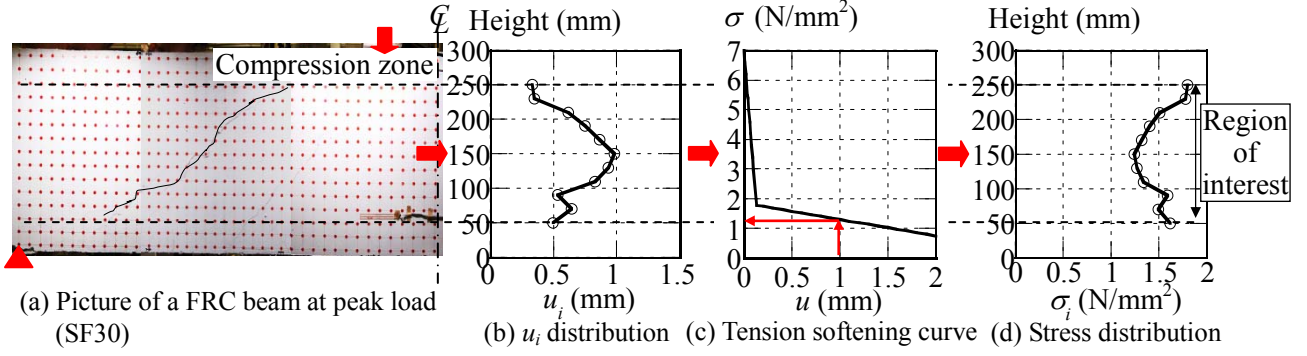


Figure 7: Investigation of tensile stress transferred across the diagonal crack

capacity of members without shear reinforcing steel (V_c), shear capacity of transverse reinforcement (V_s), and shear carried by fibers (V_f). Consequently, shear capacity (V) of FRC beams is simplified as follows:

$$V = V_c + V_s + V_f \quad (1)$$

V_c was calculated from Equation (2) by following the JSCE design specifications [9]. V_s was obtained from Equation (3). Hence the experimental value of shear carried by fibers (V_{fexp}) can be obtained from Equation (4).

$$V_c = 0.2 \cdot \sqrt[3]{f'_c} \cdot \sqrt[4]{1000/d} \cdot \sqrt[3]{100p_w} \cdot b_w \cdot d \quad (2)$$

$$V_s = A_w f_{wy} (z \cot \theta / s) \quad (3)$$

$$V_{fexp} = V_{exp} - V_c - V_s \quad (4)$$

where f'_c is the compressive strength of the concrete measured using the cylindrical specimen $\phi = 100 \times 200$ mm (N/mm²), d is effective depth (mm), p_w is longitudinal reinforcement ratio, b_w is web thickness (mm), s is stirrup spacing (mm), A_w is the total cross-sectional area of stirrups provided in the range of s (mm²), f_{wy} is the yield strength of stirrups (N/mm²), z is distance from the location of compressive stress resultant to the centroid of tension steel ($z = 7d/8$) (mm), θ is angle between the diagonal crack and horizontal line measured from the observed diagonal crack (degree) (see in Fig. 6), and V_{exp} is the experimental value of shear capacity (kN).

Furthermore, according to the JSCE design guidelines [5], the shear capacity of FRC members can be predicted by using Equation (5). Thus, the experimental value of κ ($= \kappa_{exp}$) can be calculated by Equation (6). However,

Equation (5) was proposed only for steel fiber reinforced concrete members having 1.0–1.5% fiber out of full concrete volume.

$$V_{cal} = (1 + \kappa) \cdot V_c + V_s \quad (5)$$

$$\kappa_{exp} = V_{fexp} / V_c \quad (6)$$

where V_{cal} is the predicted shear capacity (kN) and κ is the coefficient representing the effect of fibers ($\kappa = 1.0$) [5].

4.2 Method for evaluating shear carried by fibers

The authors [6] have proposed a method for evaluating shear carried by steel fibers by using tension softening curves. Tensile stress transferred across the diagonal crack (σ) can be converted from crack surface displacement (u) by using the relationship between tensile stress and crack opening displacement of the tension softening curves, as shown in Fig. 7.

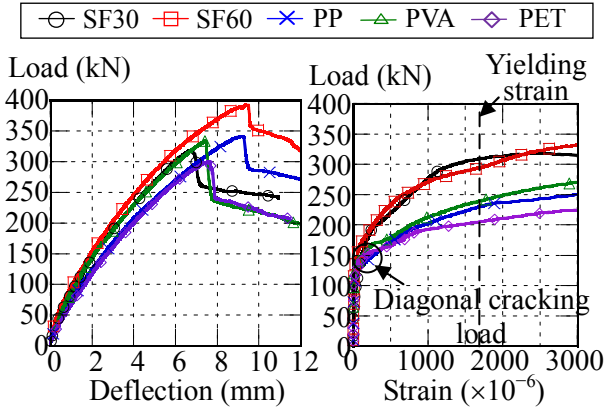
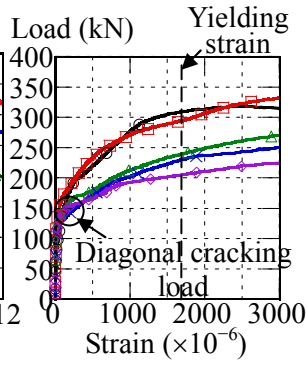
To precisely evaluate the shear carried by fibers, the specimens were divided into 15 elements with a height of 20 mm (Fig. 6), corresponding to the interval of red targets in the image analysis. Crack surface displacement (u_i), length (L_i), the angle of principal tensile strain (β_i), and the angle of the diagonal crack (θ_i) of each element were investigated.

By considering the force acting at the diagonal crack in a FRC beam due to the effect of fibers (Fig. 6), the force resisted by fibers was equal to the product of stress σ and the area of the crack surface normal to direction of σ . The stress and shear forces were calculated for each element. The force along the diagonal crack originated from the portion below the

Table 4: Summary of the calculation and experimental results

Specimen	Concrete		Results of diagonal crack				Calculation and experimental results						
	f'_c (N/mm ²)	f_t (N/mm ²)	u_{avg} (mm)	L (mm)	β_{avg} (°)	θ (°)	V_{exp} (kN)	V_c (kN)	V_s (kN)	V_{fexp} (kN)	κ_{exp}	V_{fcal} (kN)	V_{fexp}/V_{fcal}
SF30	55.3	3.05	0.67	387.3	63.3	36.8	158.8	56.3	43.0	59.5	1.06	72.6	0.82
SF60	61.9	3.69	1.08	378.3	64.6	38.2	196.3	58.4	39.6	98.3	1.68	96.2	1.02
PP	57.0	3.14	0.94	428.1	69.2	27.5	170.8	56.9	59.8	54.1	0.95	53.6	1.01
PVA	65.4	3.02	0.69	490.6	63.7	27.0	166.8	59.5	61.1	46.1	0.78	40.4	1.14
PET	51.8	2.97	0.62	427.3	64.8	31.0	149.9	55.1	51.9	43.0	0.78	43.0	1.00

f'_c : compressive strength, f_t : tensile strength, u_{avg} : average crack surface displacement at the peak, L : total crack length at the peak, β_{avg} : average angle of principal tensile strain at the peak, θ : angle between the diagonal crack and horizontal line.


Figure 8: Load-deflection curves

Figure 9: Stirrups strain curves

compression zone to the tip of the diagonal crack in the tension zone, and this zone was called the region of interest, as observed in Fig. 6. The compression zone was from the height of specimens on the top surface to the location of the neutral axis at the peak, which was calculated from displacements of targets obtained from the image analysis. The tip of the diagonal crack ended at the location of the tensile bars. In this study, the region of interest was considered to be in the range 50–250 mm from the bottom surface of the specimens.

The summation of forces in the region of interest was corresponded to shear carried by fibers. Consequently, shear carried by fibers (V_{fcal}) can be expressed as follows [6]:

$$V_{fcal} = \sum_{i=1}^n (\sigma_i \cdot b_w \cdot L_i \cdot \cos(\beta_i + \theta_i - 90) \cdot \sin \beta_i) \quad (7)$$

where n is the number of elements in the region of interest ($n = 11$), σ_i is the tensile stress of the element i (N/mm²), L_i is the length of the diagonal crack of the element i

(mm), β_i is the angle of the principal tensile strain of element i (degree), and θ_i is the angle of the diagonal crack of the element i (degree).

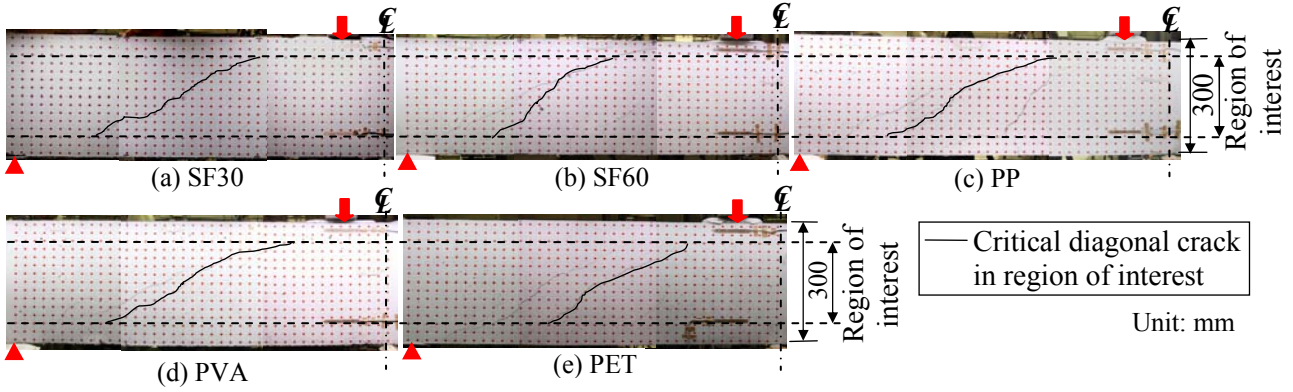
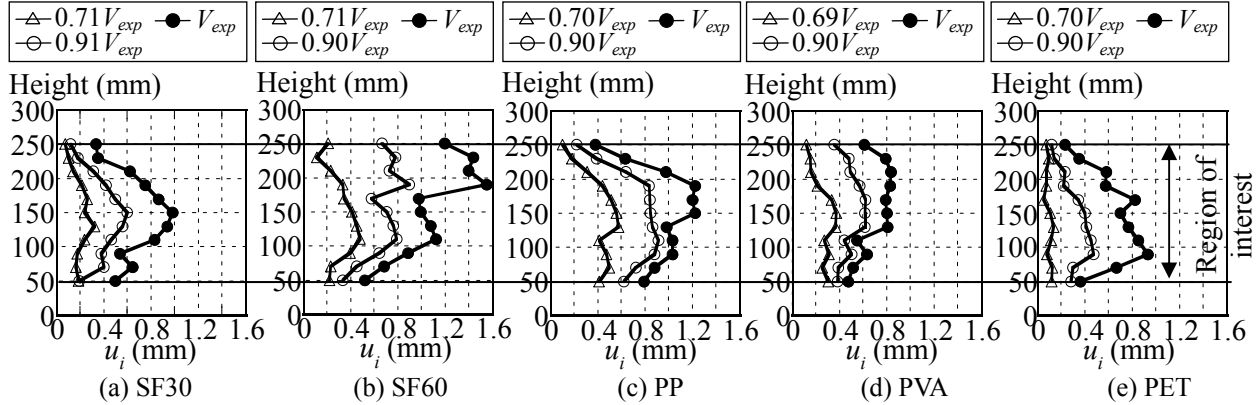
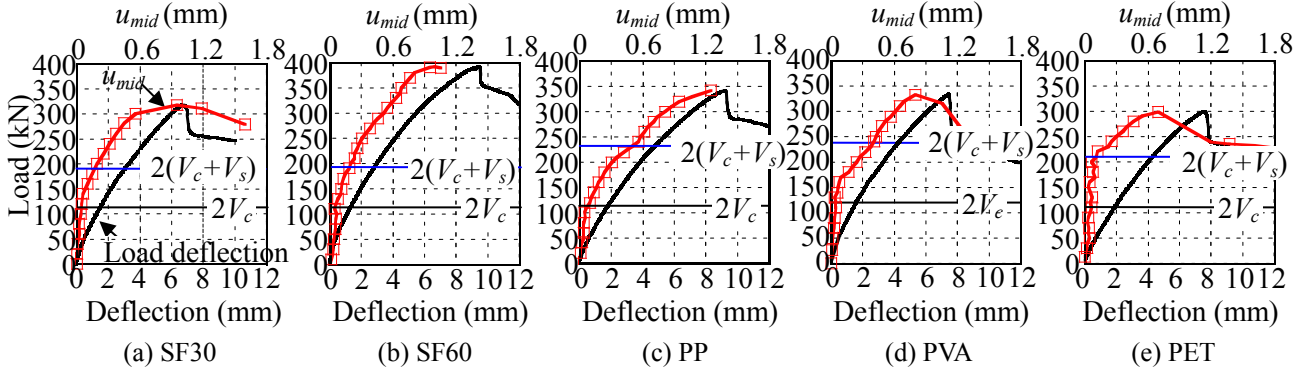
This method [6] was validated for evaluating shear carried by steel fibers having hooked ends and lengths of 30 mm, with high accuracy. However, it has not yet been extended to FRC beams with various types of fibers.

5 EXPERIMENTAL RESULTS AND DISCUSSIONS

5.1 Effect of fibers on shear behavior

The relationship between the applied load and the mid-span deflection is presented in Fig. 8. The load-deflection response was linear prior to cracking. After the initiation of the first flexural cracking, the load-deflection response became nonlinear. Later, the diagonal crack was observed in the test span, and it propagated to the loading point and support. In the pre-peak region, the propagation of the diagonal crack stopped, and the inclination of the load-deflection curve decreased. Then, diagonal tension failure occurred, and the concrete in the compression zone was crushed. The same behavior of the load-deflection response could be observed in all specimens.

Table 4 summarizes the concrete properties, information regarding diagonal cracks, calculated shear forces and shear forces obtained from the loading tests of FRC beams. The shear capacity (V_{exp}) of SF60 was the highest among all specimens. The difference in V_c between each specimen was small because the compressive strength of the


Figure 10: Crack distribution at the peak load

Figure 11: Distribution of crack surface displacement along the height of diagonal crack

Figure 12: Development of crack surface displacement and deflection

concrete did not significantly vary. On the other hand, V_s was different in each specimen due to the deviation in the angle of the diagonal crack, which was measured from the observed diagonal crack (θ in Fig. 6). The values of θ are given in Table 4. Steel fibers provided steeper angles of diagonal cracks than synthetic fibers. Figure 9 shows the average strain of stirrups in the test span. Stirrups in the test span were yielded before the ultimate load. Synthetic fibers (PP, PVA, and PET) led the early yielding of stirrups before SF30 and SF60.

Considering the shear carried by fibers, it

was found that the V_{fexp} of SF60 was the greatest, thereby resulting in the largest shear capacity. The κ_{exp} values of SF30 and SF60 were greater than 1.0, whereas those of PP, PVA, and PET were less than 1.0. Steel fibers can enhance V_{fexp} more effectively than synthetic fibers. The difference in the type of fibers caused the difference between V_{exp} , V_{fexp} as well as the load level for which stirrups were yielded.

5.2 Crack distribution along the depth

Figure 10 shows the crack distribution at the peak load. The diagonal crack was not

observed near the top and bottom fibers. This study focuses on the tensile force along the critical diagonal crack.

From the image analysis results, the value of crack surface displacement (u_i) along the height of the diagonal crack is shown in Fig. 11. Generally, the diagonal crack surface displacement was greater at approximately the middle height of specimens when compared with u_i at the top and the bottom of specimens because of the compression zone at the top of specimens and restraint by longitudinal reinforcing bars at the bottom part of the specimens. The parameter u_i rapidly increased at V_{exp} when compared with that at $0.9V_{exp}$. In addition, u_i varied depending on the types of fibers. Although the u_i of SF60 at a height of 250 mm was wide (Fig. 11(b)), the crack above the height of 250 mm was very small. To develop an identical calculation procedure for all specimens, the region of interest was in the range of heights 50–250 mm from the bottom surface of the specimens in this study.

5.3 Growth of crack surface displacement by loading

Figure 12 shows the crack surface displacements measured at the middle height of the specimens (u_{mid}), which was located 150 mm from the bottom of the specimens in the top horizontal axis, together with the load-deflection curve. In addition, the values of $2V_c$ and $2(V_c + V_s)$ were indicated in Fig. 12. The diagonal crack was generated near the load corresponding to $2V_c$. After the initiation of the diagonal crack, the values of u_{mid} linearly increased with the load. However, the increase in u_{mid} for PET was delayed because of the delayed occurrence of the critical diagonal crack. Then, u_{mid} increased drastically before the peak load. This increase corresponded to the load when the load-deflection curve started exhibiting a nonlinear behavior. Therefore, the sudden increment in u_{mid} was related to the peak, and it led to the failure of FRC beams.

5.4 Diagonal crack length

The crack length (L) is the summation of L_i in the region of interest. Table 4 listed the

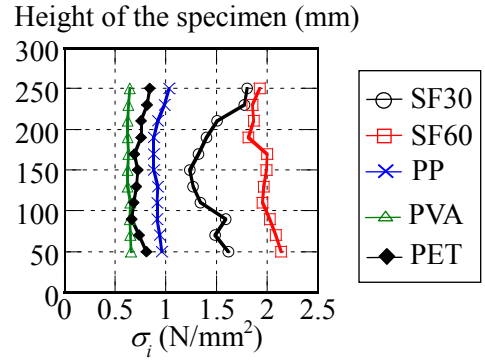


Figure 13: Distribution of u_i and σ_i at peak load

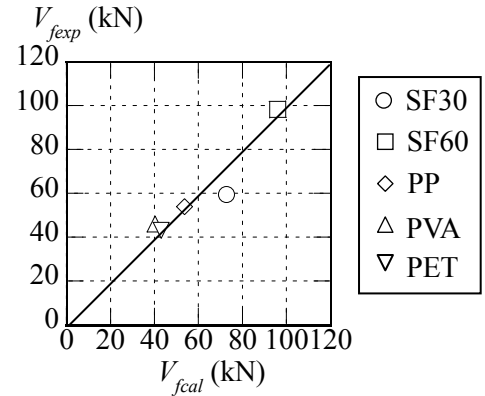


Figure 14: Comparison between V_{fexp} and V_{fcal}

crack length. PP, PVA, and PET provided longer diagonal crack lengths than those by specimens with steel fibers (SF30 and SF60), as shown in Table 4, because of the relatively flatter angle of diagonal cracks, θ .

5.5 Angles of principal tensile strain and diagonal crack

The angles of principal tensile strain (β) and diagonal crack (θ) were measured. Table 4 gives the average value of β_i in the region of interest (β_{avg}). The parameter β_{avg} did not change significantly among these specimens. On the other hand, by considering θ , the steel fibers (SF30 and SF60) revealed steeper diagonal cracks than those of synthetic fibers.

5.6 Calculated shear carried by fibers

The tensile stress transferred across the diagonal crack at the peak load was evaluated from crack surface displacement and the relationship between the tension softening curves listed in Table 3, as mentioned in Section 4.2. The stresses across the diagonal

crack in FRC beams at the peak load are shown in Fig. 13. The larger stress could be resisted to the top and bottom parts of the specimens because of the smaller u_i . SF60 can resist the highest stress, thereby resulting in the largest V_{fexp} , whereas PP, PVA, and PET resisted relatively lower stresses across the diagonal crack.

Shear carried by the fibers (V_{fcal}) was calculated using Equation (7) and was summarized in Table 4. Figure 14 shows the comparison between the experimental results and calculated values. The ratio of the mean of the experimental value to the calculated value of shear carried by fibers was 1.00 with a coefficient of variation (C.V.) of 11.6%.

The proposed method can be used to evaluate shear carried by fibers of FRC beams. Moreover, this method can be used when the material types and lengths of fibers were varied because the tension softening curves can reflect the characteristic of each fiber. The application of these curves to examine the stress transferred across the diagonal crack of FRC beams was proven.

6 CONCLUSIONS

- (1) Shear capacity of FRC beams with 60-mm steel fibers was the greatest when compared with a specimen having 30-mm steel fibers, polypropylene, polyvinyl alcohol, or polyethylene terephthalate because of the best post-cracking behavior in the tension.
- (2) The value of crack surface displacements of FRC beams varied depending on the type of fibers. However, the distribution of crack surface displacement along the diagonal crack was similar because the crack surface displacement near the middle height of FRC beams was greater than those at the top and bottom of specimens. In addition, crack surface displacement significantly widened just before the peak load. This behavior can be observed in all specimens regardless of the fiber type.
- (3) The specimen with 60-mm steel fibers provided the widest crack surface

displacement at the peak load because of the effects of the fiber length and shape of ends. However, it was most effective for transferring stress across the crack because it could resist the highest stress in post-cracking behavior, as indicated by the tension softening curve. Therefore, the post-cracking behavior in the curve is essential for investigating the shear resisting mechanism of FRC beams.

- (4) By considering an identical crack surface displacement, steel fibers can transfer more stress across the diagonal crack than that by synthetic fibers, thereby resulting in the higher shear transferred force by fibers.
- (5) The method to evaluate the shear contribution of fibers was presented. The calculated shear carried by fibers showed a good agreement with experimental results, even for various material types and fiber lengths.

ACKNOWLEDGMENT

The authors acknowledge the support received from the Center for Urban Earthquake Engineering (CUEE) of Tokyo Institute of Technology.

REFERENCES

- [1] Kwak, Y.-K., Eberhard, M. O., Kim, W.-S. and Kim, J., 2002. Shear strength of steel fiber-reinforced concrete beams without stirrups. *ACI Structural Journal*. **96**(4):538-530.
- [2] Narayanan, R. and Darwish, I. Y. S., 1987. Use of steel fibers as shear reinforcements. *ACI Structural Journal*. **84**(3):227-216.
- [3] Sharma, A. K., 1986. Shear strength of steel fiber reinforced concrete beams. *ACI Structural Journal*. **83**(4):628-624.
- [4] Li, V. C., Ward, R. and Hamaza, A. M., 1992. Steel and synthetic fibers as shear reinforcement. *ACI Materials Journal*. **89**(5):508-499.

- [5] Japan Society of Civil Engineers (JSCE), 1999. *Guidelines of design for RSF piers; Concrete Library 97*. JSCE. (in Japanese)
- [6] Jongvivatsakul, P., Watanabe, K., Matsumoto, K. and Niwa, J., 2011. Evaluation of shear carried by steel fibers of reinforced concrete beams using tension softening curves. *Journal of Materials, Concrete Structures and Pavements, JSCE*. **67**(4):507-493.
- [7] Watanabe, K., Higashi, H. and Niwa, J., 2009. Real-time image analyzing system for evaluating the shear failure mechanism of reinforced concrete beams. *The 4th International Conference on Construction Materials: Performance, Innovations and Structural Implications (ConMat'09)*, Aug. 24-26, 2009, Nagoya, Japan; pp.1482-1477.
- [8] Japan Concrete Institute (JCI), 2003. *Method of Test for Fracture Energy of Concrete by Use of Notched Beams*. JCI.
- [9] Japan Society of Civil Engineers (JSCE), 2010. *Standard specifications for concrete structures-2007, Design*. JSCE. http://www.jsce.or.jp/committee/concrete/e/JGC15_Standard%20Specifications_Design_1.0.pdf. (Accessed date: Aug. 23, 2012)